Modelling of Zircaloy-4 accelerated degradation kinetics in nitrogen-oxygen mixtures at 850°C

Marina Lasserre, Véronique Peres, Michèle Pijolat, Olivia Coindreau, Christian Duriez, Jean-Paul Mardon

Modelling of Zircaloy-4 accelerated degradation kinetics in nitrogen-oxygen mixtures at 850°C

M. Lasserre [1, 2, a], V. Peres [2], M. Pijolat [2, b], O. Coindreau[1], C. Duriez[1], J.-P. Mardon [3]

[1] Institut de Radioprotection et de Sûreté Nucléaire, Cadarache BP 3, 13 115 St Paul-Lez-Durance cedex, France

[2] Laboratoire George Friedel CNRS UMR 5307, Centre SPIN, Département PRESSIC, Ecole Nationale Supérieure des Mines, 158 Cours Fauriel, 42 023 Saint-Etienne, France

[3] AREVA, AREVA NP SAS Fuel Business Unit, 10 rue Juliette Récamier, 69 456 Lyon Cédex 06, France

Keywords: Zircaloy-4; thermogravimetry; high temperature corrosion; oxygen-nitrogen mixture

[a] Present address : EDF – DPI – DAIP – UFPI
Service Formation de Civaux
BP 64
86 320 Civaux
Tel.: +33549834129; e-mail address: marina.lasserre-gagnaire@edf.fr

[b] Corresponding author : Tel. :+33477420152 ; fax :+33477499694 ; e-mail address : mpijolat@emse.fr

Modelling of Zircaloy-4 accelerated degradation kinetics in nitrogen-oxygen mixtures at 850°C

M. Lasserre [1, 2, a], V. Peres [2], M. Pijolat [2, b], O. Coindreau[1], C. Duriez[1], J.-P. Mardon [3]

[1] Institut de Radioprotection et de Sûreté Nucléaire, Cadarache BP 3, 13 115 St Paul-Lez-Durance, France

[2] Laboratoire George Friedel CNRS UMR 5307, Centre SPIN, Ecole Nationale Supérieure des Mines, 158 Cours Fauriel, 42 023 Saint-Etienne, France

[3] AREVA, AREVA NP SAS Fuel Business Unit, 10 rue Juliette Récamier, 69 456 Lyon Cédex 06, France

Abstract

Zirconium-based alloys used in PWR cladding show an acceleration of their oxidation kinetics in air at high temperature compared to their behaviour under oxygen or steam alone. This paper presents an analysis of the oxidation kinetics in order to explain the role of nitrogen during the accelerated corrosion. Isothermal thermogravimetry on alloy thin plates was used to collect kinetic data during the reaction of Zircaloy-4 at 850°C in oxygen and nitrogen mixtures. The influence of oxygen and nitrogen partial pressure on the degradation kinetics was studied by a jump method. The presence of nitrogen in the reacting gas enables the formation of zirconium nitride near the oxide-metal interface which acts as a catalytic phase. A three steps reaction path composed of nitride oxidation, α-Zr(O) nitridation and oxidation is proposed. A detailed mechanism and the rate-determining step of the overall process are proposed that account for the experimentally observed dependence of the kinetic rate with the oxygen and nitrogen partial pressures; a kinetic model based on surface nucleation and growth of regions attacked by nitrogen was successful in describing the mass variations with time of exposure at 850°C.

1. Introduction

Exposure of fuel cladding material to air or air - steam mixture may occur in case of a core meltdown accident with subsequent reactor pressure vessel breaching in a nuclear reactor. It could also happen under shutdown conditions in case of dewatering during assemblies handling, in spent fuel storage pools after accidental loss of cooling and dewatering of the assemblies, as well as in storage and transportation cask accidents. Previous studies have shown that high temperature oxidation of pure Zr or of Zr-based alloys is much faster in atmospheres containing nitrogen (mixed with oxygen and/or steam) than in nitrogen-free atmospheres [1]-[9]. Nitrogen is thus observed to strongly influence the Zr oxidation mechanism when present in the reacting gas. However, no significant direct reaction between pure nitrogen and zirconium could be observed in the temperature range of interest [6]. Below about 1050°C, oxidation of zirconium alloys, which has been studied extensively in the past five decades, exhibits a kinetic transition (corresponding to an increase in the oxidation rate) concomitant with a degradation of the first formed dense zirconia layer grown during the pre-transition stage. The origin of the kinetic transition itself has been a matter of debate among numerous authors and will not be discussed hereafter. Nitrogen in the oxidant atmosphere has been found to have no significant effect on the kinetic in the pre-transition, diffusion-driven regime, but was observed to strongly shorten the pre-transition duration of this regime and to enhance the oxidation rate in the post-transition stage [5][6][10].

The accelerating effect of nitrogen is still not well understood. Rosa et al. [3] have proposed that nitrogen dissolves into the pre-transition oxide which leads to the formation of ZrN precipitates close to the metal-oxide interface; their subsequent oxidation into zirconia provokes cracks due to the molar volume change and subsequent free access of the reacting gas to the metal surface. The same sequence of events would be responsible for the kinetic transition and the fast degradation in the post-transition stage as well, until the metal is entirely consumed. More recently, Duriez et al. [5] and Steinbruck et al. [6] proposed that local oxygen starvation consecutive to the appearance of cracks in the pre-transition zirconia layer favours the formation of the ZrN compound at the bottom of cracks. ZrN is then oxidised by fresh air flowing from the external surface, and again the ZrN to ZrO_2 conversion creates cracks in the growing oxide. Usually, attack is localized and porous zirconia nodules extend progressively, laterally and inwards.

Both mechanisms can explain formation of a highly porous zirconia, co-existing with a low amount of zirconium nitride precipitates, mainly located close to the metal/oxide interface. However, zirconia is the final product of the reaction, in accordance with thermodynamical considerations (at 850°C in ≈ 100000 kPa of nitrogen, the ZrO_2-ZrN equilibrium oxygen pressure is less than 10^{-25} kPa [10]).

Most of the studies on the nitrogen effect were done in air, so that the effects of the respective partial pressures of oxygen and nitrogen on the kinetics have not yet been determined. Moreover, observation of the oxidised samples often revealed that the corrosion layer is not uniformly spread over the entire sample surface, and since these studies were performed with tube segments, it raises questions about the gas dynamics and the local partial pressures in the vicinity of the sample surface.

For better analytical understanding of the Zr-alloy oxidation mechanisms in presence of nitrogen, it was decided to get reliable kinetic data using small Zircaloy-4 plates and to study separately the effect of the partial pressure of both gases. In a previous article [10], the morphological changes of the samples reacting in oxygen-nitrogen mixtures at 850°C investigated by optical metallography and scanning electron microscopy were described. A 850°C temperature was chosen since it enables the observation of the accelerated kinetic regime over a period of time long enough for minimizing temperature and partial pressure gradients in the reacting system. A detailed analysis of the reactions to consider was made to account for the nature of the observed phases and the interfaces between them, as well as their spatial distribution inside the attacked regions. The scenario proposed was based on the formation of ZrN precipitates during the pre-transition stage, inducing a random appearance of attacked regions, whose number was found to vary with the partial pressure of both gases; inward progression of the attacked regions forms growing nodules and is the main process observed during the accelerated post-transition stage. The present paper attempts to quantify these processes and proposes a kinetic model and a mechanism in order to obtain a predictive rate law and the key parameters governing the reaction kinetics.

2. Experimental

2.1. Samples

A sheet of Zircaloy-4, whose chemical composition is given in Table 1, was provided by AREVA-NP and the samples were cut to 10 mm x 10 mm for the thermogravimetry tests. The

thickness was equal to 450 µm which enables to minimize the mass gain due to the edges compared to that due to the plane faces. The bare plates were cleaned in acetone and dried before each experiment.

Alloy	Sn (wt. %)	Fe (wt. %)	O (wt. %)	Cr (wt. %)	C (wppm)	Nb (wppm)	H (wppm)
Zircaloy-4	1.32-1.35	0.21	0.123-0.129	0.11	125-140	< 40	< 3

Table 1. Composition of the Zircaloy-4 alloy investigated.

2.2. Thermogravimetry tests

Corrosion kinetics in O_2-N_2-He flowing mixtures was followed by means of a symmetrical high precision thermobalance (SETARAM-TAG24). The sample was hanged to a quartz rod, whereas an alumina plate with the same dimensions was placed in the reference furnace in order to minimise baseline shift during experiments (see Figure 1). Total flow rate passing over the sample was fixed to 6 $L.h^{-1}$ which was sufficient to avoid kinetic limitations in the gas phase. O_2 and N_2 partial pressures were adjusted to the desired values thanks to mass flow meters, the total pressure being equal to the atmospheric pressure.

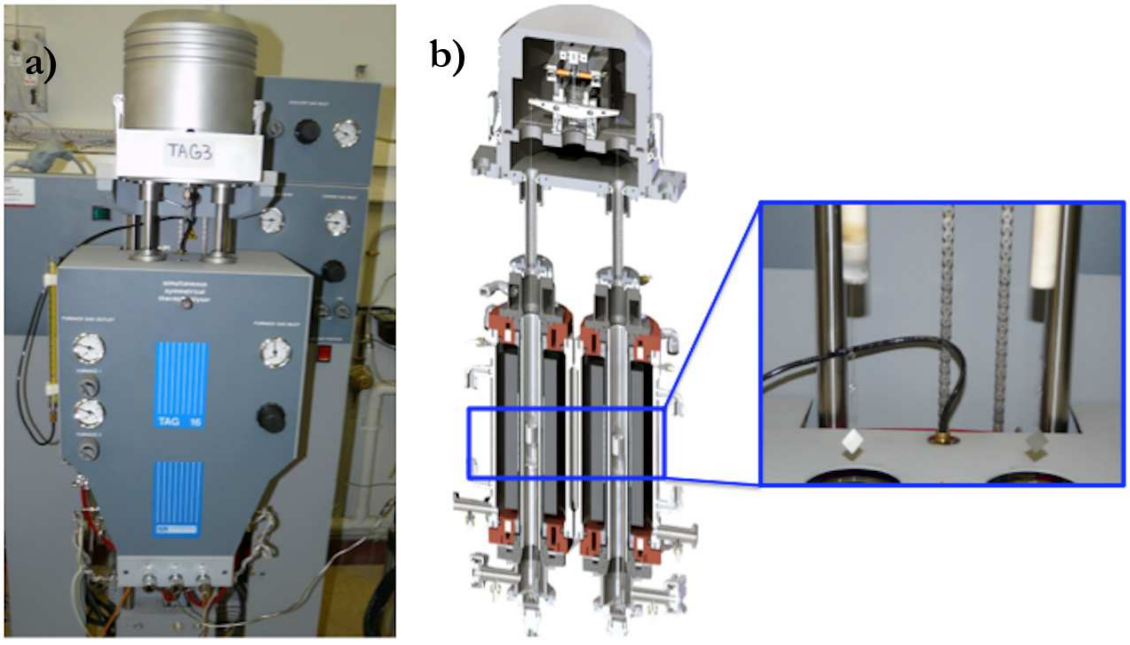

Fig. 1. Thermobalance SETARAM-TAG24. Picture of the equipment (a) and device overview with a picture of the hanged sample (b).

For all experiments, the desired reactive gaseous mixture was introduced at ambient temperature, then the temperature was raised at a rate of 10°C.min^{-1} up to 850°C and maintained at this temperature during several hours. Previous tests done by introducing the reacting gas at 850°C just after the temperature ramp under helium showed non reproducible curves even in the pre-transition stage [10].

During some experiments, temperature jumps or oxygen or nitrogen partial pressure jumps were done in order to quantitatively evaluate the kinetic response of the reacting sample to an abrupt change of one of the thermodynamic variables. Temperature jumps were done from 850 to 830°C. Time necessary for temperature to reach a constant value after the jump did not exceed 180 s. Jumps in oxygen or nitrogen partial pressures were achieved by modifying the corresponding mass flow rate. Helium flow rate was simultaneously changed in order to keep constant the total flow rate without changing the partial pressure of the other reacting gas. Time necessary for the partial pressures to reach a constant value after the jump did not exceed 360 s.

3. Results

3.1. Steady-state approximation

As seen in the introduction section, it is clear that the system under study is very complex; so before attempting any kinetic modelling, it was necessary to verify the existence of a steady state during the experiments, which is one of the key approximations used in the kinetic analysis of gas-solid reactions. According to Pijolat et al. [11], this verification may be done thanks to the coupling of thermogravimetry and calorimetry which offer two simultaneous ways of measuring the kinetic rate of a reaction. In such an experiment, the quartz rods were replaced by a differential scanning calorimetry (DSC) rod in one furnace and by a phantom rod in the other furnace. Figure 2 represents the mass gain (expressed in g.m^{-2}) as a function of time during an experiment in 20% O_2 - 80% N_2 atmosphere. The vertical dotted line corresponds to the beginning of the isothermal and isobaric conditions. The mass gain rate versus time obtained by time derivation of the curve of Figure 2 is plotted in Figure 3 (continuous line). Once isothermal and isobaric conditions are reached, the mass gain rate (also called the reaction rate) decreases, which corresponds to the pre-transition stage. Then, the reaction rate passes through a minimum before the accelerated post-transition stage. As expected, the reaction rate increases during the post-transition stage. The dotted line in Figure

3 is the measured heat flow (*dQ/dt*) which is seen to follow exactly the mass gain derivative curve.

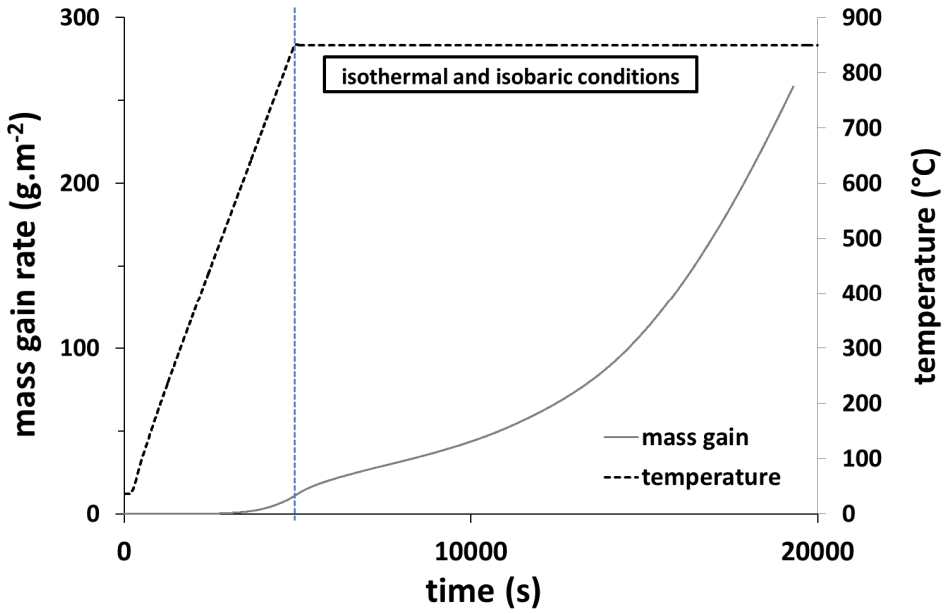

Fig. 2. Mass gain versus time at 850°C of Zircaloy-4 in 20% O_2 - 80% N_2 atmosphere at 850°C.

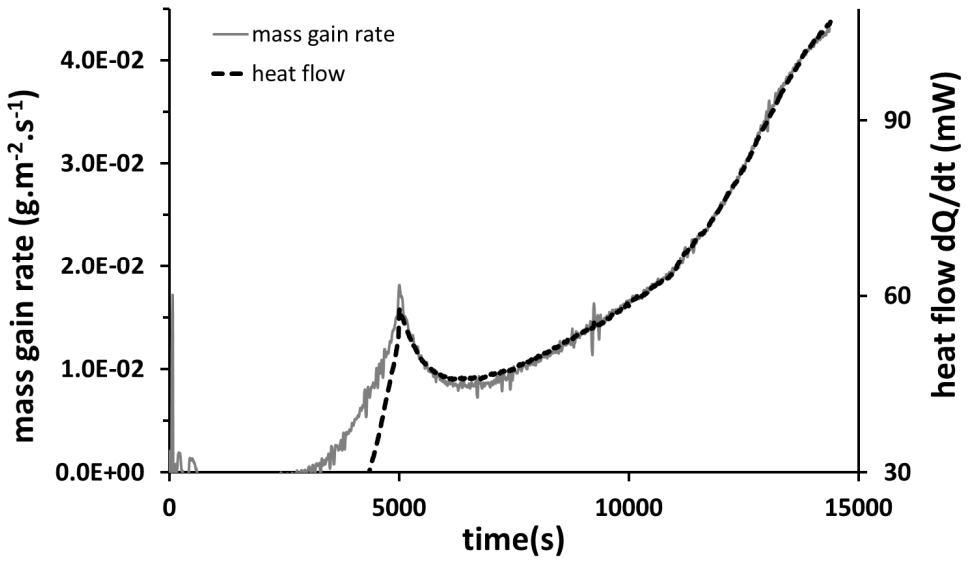

Fig. 3. Mass gain rate (850°C, P_{O2} = 20 kPa, P_{N2} = 80 kPa) and heat flow versus time.

The steady state approximation is valid if both rates are linked by a linear relationship according to the following equation [11]:

$$\frac{dQ}{dt} = \frac{-\Delta H}{\sum_G \nu_G M_G} \frac{d\Delta m}{dt} \qquad \text{(Eq. 1)}$$

Where dQ/dt is the heat flow (in $J.s^{-1}$), ΔH is the enthalpy of reaction (in $J.mol^{-1}$), M_G is the molar mass of gas G involved in the reaction balance (in $g.mol^{-1}$), ν_G is the algebraic stoichiometric number of gas G entering in the reaction balance and $d\Delta m/dt$ is the mass gain rate (in $g.s^{-1}$).

Figure 3 shows that both rate curves are well superimposed during all the accelerated stage indicating that the steady-state test is established during the post-transition stage in such conditions. Similar experiment done with 5% O_2 - 5% N_2 in helium at the same temperature gave the same result [10][12], thus it can be extrapolated that at 850°C the reaction during the post-transition stage progresses in steady state conditions whatever the oxygen and nitrogen partial pressures.

3.2. Rate-determining step

Another essential approximation for the kinetic modelling of solid-gas reactions is the existence of a rate-determining step which controls the overall reaction rate and, given that the mechanism of reaction can be decomposed into a set of elementary steps, it allows expressing the reaction rate from the rate of a single elementary step. This approximation can be verified using the sudden change (or jump) method as already shown for various reacting systems [11]. When the kinetics is governed by a single rate-determining step, it can be shown that the mass gain rate due to zirconium oxidation into ZrO_2 can be decomposed in a product of several terms, as in Equation 2:

$$\frac{d\Delta m}{dt} = n_0 \, M_{O_2} \, \phi(T, P_i) \, S_m(t) \qquad \text{(Eq. 2)}$$

where $\phi(T,P_i)$ is the areic growth rate of zirconia (in $mol.m^{-2}.s^{-1}$) defined as the amount of reactant transformed per square meter per second, $S_m(t)$ is a function of time related to the dimensions of the zone where the rate-determining step of zirconia growth takes place (in

$m^2.mol^{-1}$), n_0 is the amount of zirconium in the initial sample (in mol), and M_{O2} is the molar mass of dioxygen (in $g.mol^{-1}$). The function $S_m(t)$ depends also of variables such as the shape and the dimensions of the solid. It can be seen in Equation 2 that the thermodynamic variables T and P_i are separated from the time variable. The method for testing the existence of a rate-determining step has been described in [11]. It is based on the comparison of the ratios of the reaction rates measured after and before the jump for several extents of reaction, i.e for several mass gains.

Due to the variables separation in $\phi(T,P_i)$ and $S_m(t)$ functions, the rate ratio reduces to that of the $\phi(T,P_i)$ terms provided that the jump is sufficiently fast to avoid mass increase during the jump (for minor morphological changes, the $S_m(t)$ function does not vary during the jump). Thus, repeating the experiment at various extents of reaction, the measured rates ratios must keep a constant value. The results are shown in Figure 4 in which the ratios measured during the post-transition stage for different mass increases for temperature jumps from 850°C to 830°C have been plotted. It can be seen that the ratios are constant and equal to 0.88 ± 0.03.

Similar experiments conducted in 5% O_2 - 5% N_2 - 90% He (850°C to 830°C jumps) showed again a constancy of the ratios during the post-transition stage, with a value of 0.82 ± 0.08.

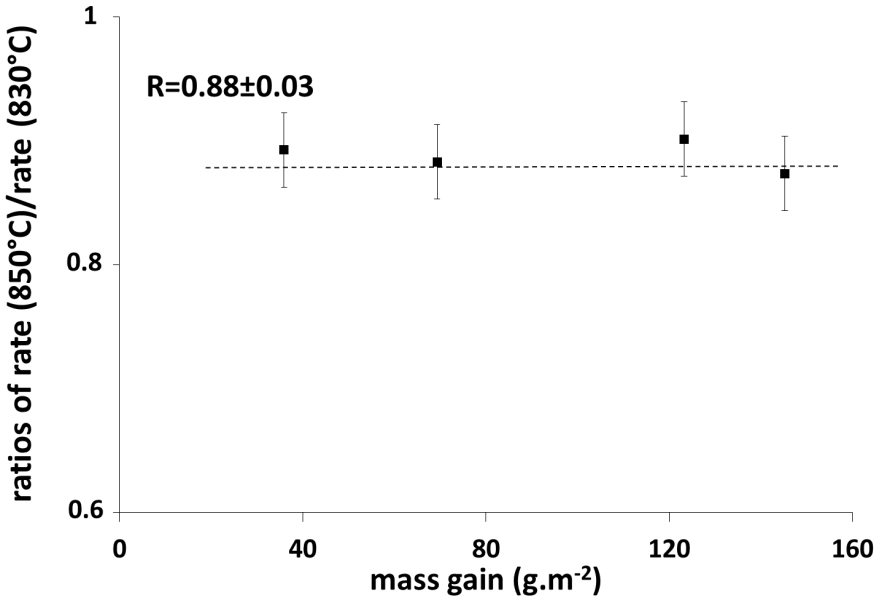

Fig. 4. Ratios of rates before and after the temperature jump from 850°C to 830°C (P_{O2} = 20 kPa, P_{N2} = 80 kPa)

3.3. Influence of oxygen and nitrogen partial pressures

According to Equation 2, partial pressure jumps of one gas while keeping constant the temperature and partial pressure of the other gas allows determination of the areic growth rate variations with partial pressure. The method relies on a series of experiments which begin in the same experimental conditions (temperature, oxygen and nitrogen partial pressures). Once a desired mass gain is reached, a partial pressure jump of one of the two gases is applied. It is illustrated in Figure 5(a), showing the evolution of the mass gain and in Figure 5(b) where the evolution of the mass gain rate is plotted. Varying the final partial pressure value from an experiment to another one and measuring the rates ratios (after to before the jump) led to the plots of Figures 6 and 7 which show the variations $\phi(T,P_i)/\phi(P_0)$ with oxygen and nitrogen partial pressure, respectively, P_0 being the partial pressure before the jumps. The advantage of this method is to provide directly the variations of the reaction rate with the partial pressure of each gas separately without any assumption on the kinetic model.

The oxygen partial pressure jumps were done at a mass gain equal to 100 $g.m^{-2}$ with initial oxygen and nitrogen partial pressures conditions corresponding to 20% O_2 - 80% N_2 whereas those in nitrogen partial pressure were done at a mass gain equal to 80 $g.m^{-2}$. In this last case, the initial conditions before jumps were 20% O_2 – 5% N_2 – 75% He. The uncertainty on the ratio determination was estimated by repeating several times the same jump experiment, and this was done for several jump amplitudes. It can be deduced from Figures 6 and 7 that oxygen partial pressure has an important influence on the $\phi(T, P_i)$ function in the range of 1 to 20 kPa whereas nitrogen has no influence on it. Moreover, the ϕ function appears to be non-affected by N_2 partial pressure variations in the range of 5 to 80 kPa.

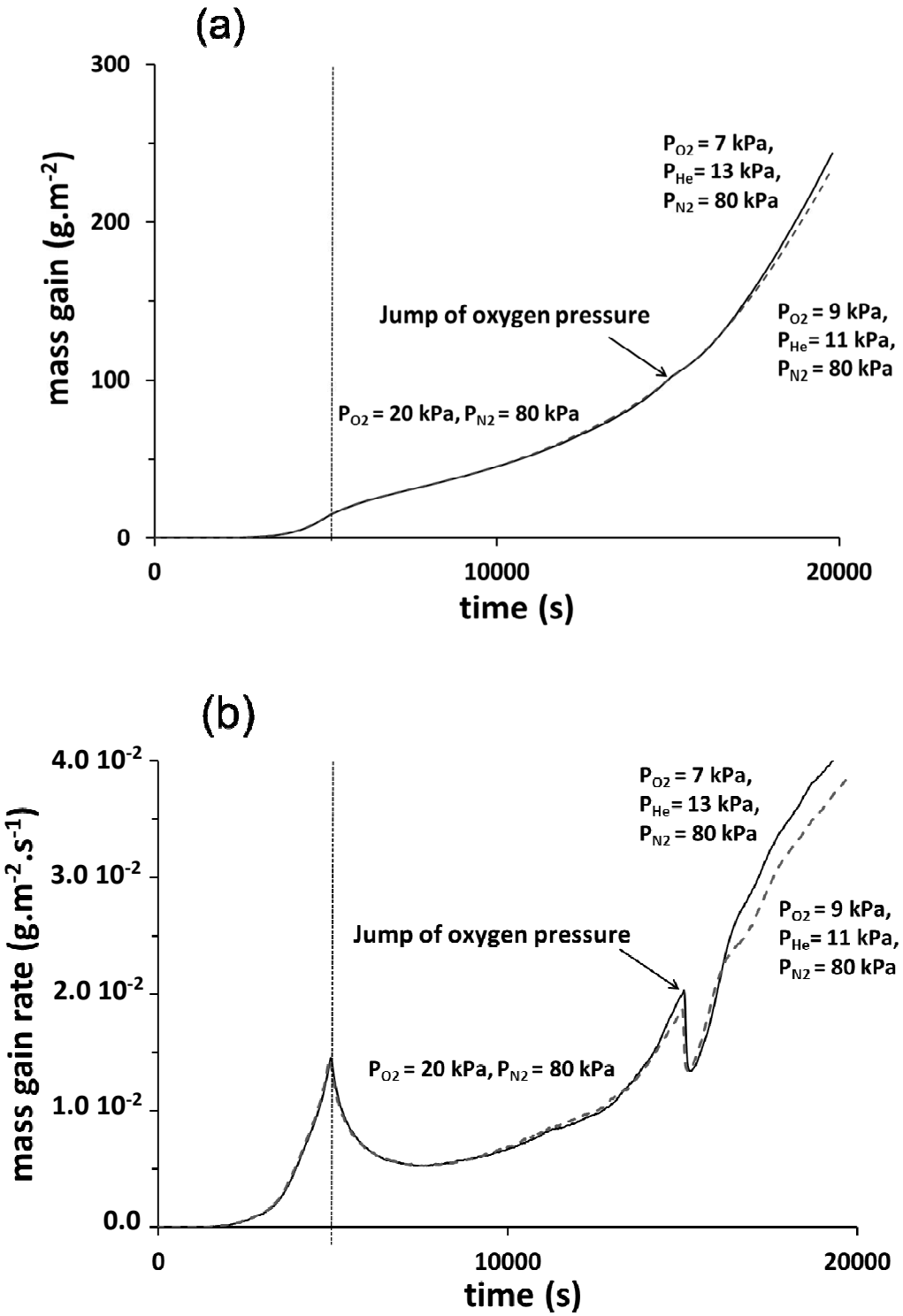

Fig. 5. Jumps of oxygen pressure from 20 kPa to 7 kPa or 9 kPa after 100 g.m^{-2} mass gain at 850°C. Mass gain curves (a) and mass gain rate curves (b).

It could be noticed that increasing the oxygen partial pressure or decreasing the nitrogen pressure during a jump induced oscillations in the reaction rate making impossible the calculation of the ratios. The origin of such oscillating regimes was not easy to understand; referring to oscillating reactions in heterogeneous systems [13], the conditions for such a behaviour are systems reacting far from equilibrium in which successive reactions involve autocatalytic effects. We will see in the following proposed interpretations that these conditions may be fulfilled.

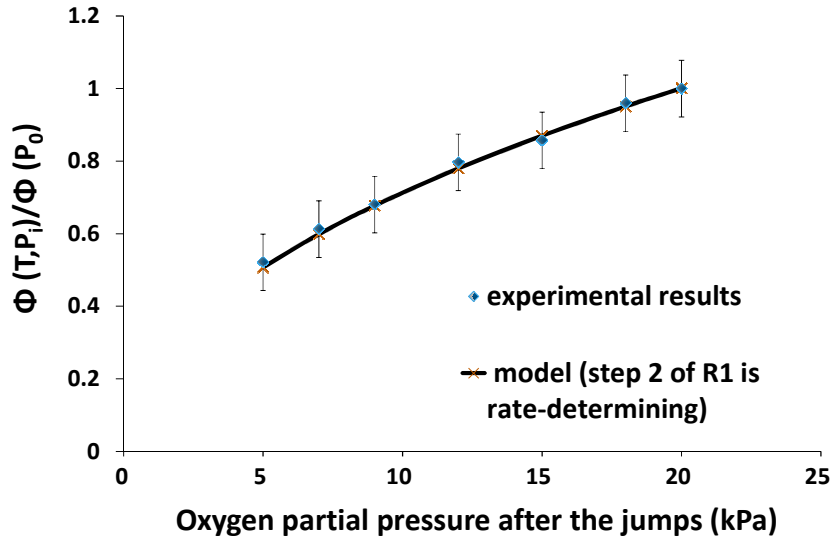

Fig. 6. Variation of $\phi(T,Pi)/\phi(P_0)$ as a function of oxygen final partial pressure at 850°C (initial conditions: P_{O2} = 20 kPa, P_{N2} = 80 kPa). Experimental data (dots) and calculated values (continuous line) using the ϕ_2 function given in table 4 (see section 4.2).

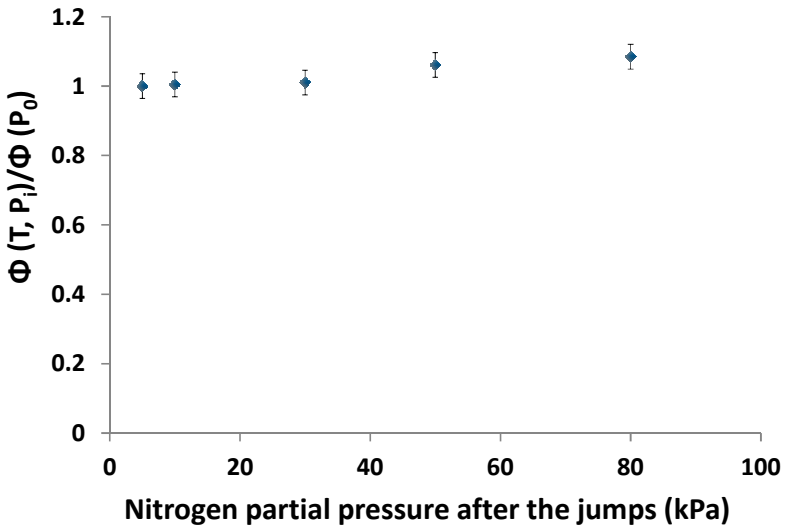

Fig. 7. Variation of $\phi(T,Pi)/\phi(P_0)$ as a function of nitrogen final partial pressure at 850°C (initial conditions: P_{O2} = 20 kPa, P_{N2} = 5 kPa, P_{He} = 75 kPa).

4. Discussion

The results presented in section 3.2 clearly show that despite of its complexity, the accelerated post-transition stage during the reaction between Zircaloy-4 and O_2-N_2 mixture at 850°C is kinetically controlled by a single rate-determining step. Rigorously, it could have been deduced from this result that during this stage the corrosion progresses according to a steady-state, and this was confirmed by the result shown in section 1. As a consequence, the reaction rate can be written as a product of several terms (see Equation 2) involving functions ϕ and $S_m(t)$. The determination of functions ϕ and $S_m(t)$, that account for the variations of the reaction rate vs. thermodynamic variables and time, respectively, is achieved in the next paragraph.

4.1. Modelling of the $S_m(t)$ and ϕ functions

It was previously reported that the kinetic curves during the accelerated period were not reproducible [10]. Equation 2 indicates that the issue comes from the $S_m(t)$ function since during the experiments temperature and partial pressures were kept constant. According to literature [5] and to our observations of partially oxidized samples (see for example Figure 8 and [10]), the acceleration corresponds to the appearance and progress of localized nodules where breakaway of the first formed dense oxide scale has occurred.

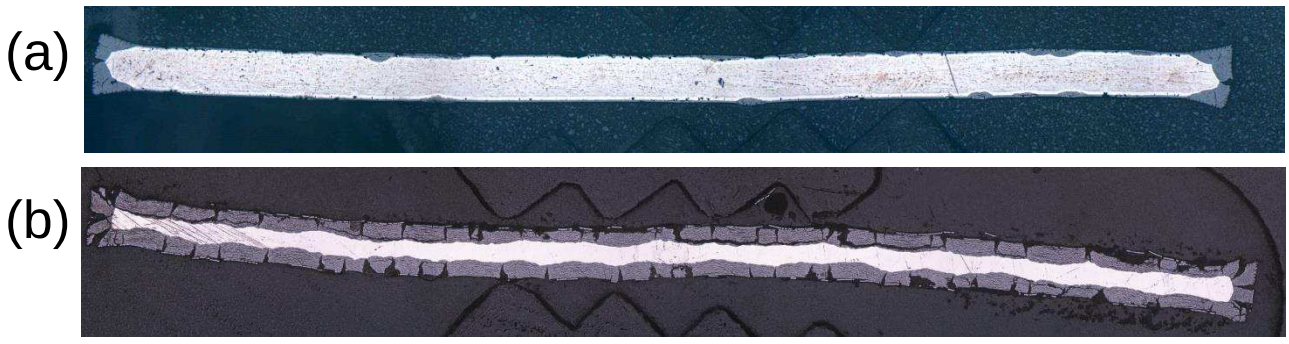

Fig. 8. Micrographs of Zircaloy-4 samples after oxidation in 20%O_2 - 80%N_2 (a) and 5%O_2 - 5%N_2 - 90%He (b) up to a mass gain of 70 and 350 g.m^{-2}, respectively.

Considering a random appearance of the nodules followed by their inward growth, analogy can be made with nucleation and growth processes observed in chemical reactions of powder material. The kinetic model best suited to quantitatively describe this kind of transformation (surface nucleation and growth) was first reported by Mampel for spherical particles [14] then by Delmon in the case of cylinders and plates [15]. Calculation of the mass gain rate due to the nucleation and growth of the nodules requires the following assumptions: (i) the probability of nucleation is uniform over the whole surface, (ii) the areic nucleation frequency is constant at constant temperature and constant partial pressures (our conditions), (iii) the growth of post-transition regions is isotropic (spherical nodules), (iv) the rate-determining step of growth is located at the nodule/metal interface.

Considering the planar symmetry of the samples and neglecting the transformation along the edges, the equations describing the variations of the S_m function vs. time during the post-transition stage can be calculated according to Delmon's mathematical treatment (cf. Appendix A, Table A). It will be demonstrated in section 4.2. that the nodules growth mechanism corresponds to a set of reactions for which the rate-determining step is located at the oxide/metal interface, according to Mampel's assumptions. Moreover, the fraction of the surface still not affected by the growing nodules can be computed according to the equations given in Appendix B, Table B.

Once the first nodule has appeared, the oxide layer is made of two co-existing regions: those still in the pre-transition stage (dense zirconia) and those already in the post-transition stage (nodules). The reaction rate is thus the sum of two terms, one is due to the growth of still non attacked dense zirconia, parallel to the interface and the other one is due to the nodules nucleation and isotropic growth:

$$\left[\frac{d\left(\Delta m/S\right)}{dt}\right]_{tot} = \left[\frac{d\left(\Delta m/S\right)}{dt}\right]_{pre} \frac{S_L(t)}{S} + \left[\frac{d\left(\Delta m/S\right)}{dt}\right]_{post} \qquad \text{(Eq. 3)}$$

where S is the initial surface area of the sample (in m^2) and $S_L(t)$ is the surface area of the sample (in m^2) still not affected by the growing nodules (the expression of $S_L(t)/S$ is reported in Appendix B, Table B).

The contribution of each term of Equation 3 can be seen on Figure 9. The mass gain rate due to the growth of dense zirconia decreases with time whereas the mass gain rate due to nodules

growth increases. The following sections are devoted to the calculation of both terms of Equation 3 making use of experimental rate curves.

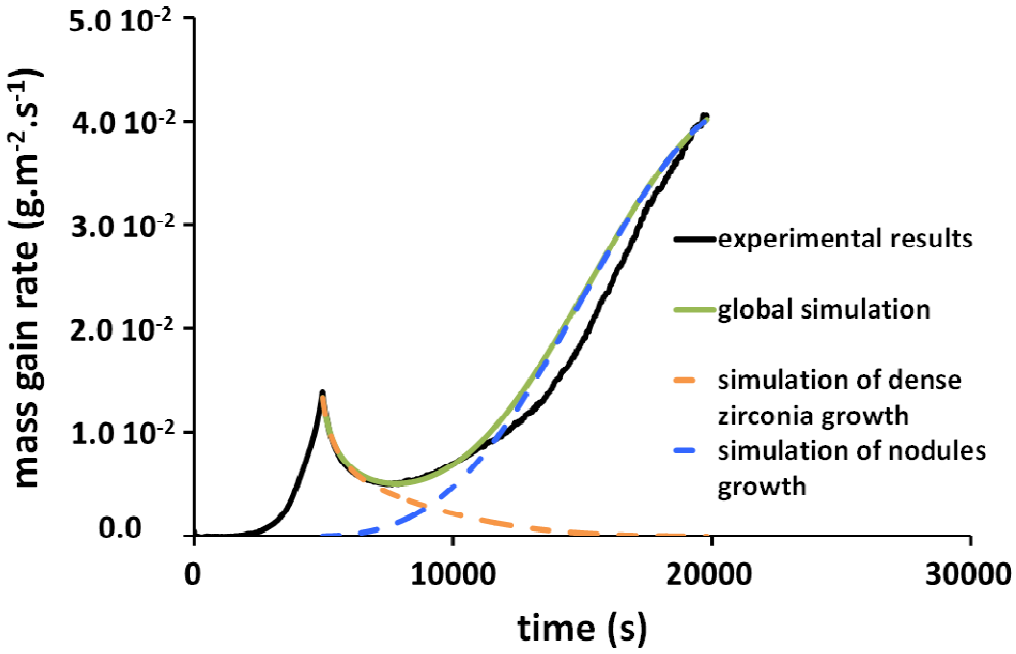

Fig. 9. Mass gain rate (850°C, P_{O2} = 20 kPa, P_{N2} = 80 kPa) versus time: experimental results and simulation results.

Growth kinetics of dense zirconia

In the pre-transition stage, it is admitted that diffusion of oxygen vacancies in the dense oxide governs the oxidation kinetics. However, the reaction rate does not strictly follow a parabolic law, but rather a "sub-parabolic" one. In previous studies ([16] , [17], [18]), it was suggested that this is due to a random distribution of barriers in the diffusion layer. The reaction rate can then be modeled by Equation 4 where the function of time $S_m(t)_{pre}$ is given by Equation 5:

$$\left[\frac{d\left(\Delta m / S\right)}{dt}\right]_{pre} = \frac{n_0 M_{O2}}{S}\phi_{pre} S_m(t)_{pre} \qquad \text{(Eq. 4)}$$

$$S_m(t)_{pre} = \frac{S}{n_0}\frac{l_0}{X}\exp[-bX] \qquad \text{(Eq. 5)}$$

ϕ_{pre} is the areic growth rate of dense zirconia (in mol.m^{-2}.s^{-1}), $X = \frac{\Delta m}{S}\frac{V_m(ZrO_2)}{M_{O2}}$ where $V_m(ZrO_2)$ is the molar volume (in m^3.mol^{-1}) of the dense zirconia and b is the number of barriers per unit length (in number.m^{-1}). The best fit between experimental curves and Equation 4 has been obtained with the values of ϕ_{pre} and b reported in Table 2 (for experiments conducted in 20% O_2 – 80% N_2 and 5% O_2 – 5% N_2 – 90% He mixtures at 850°C). Only the decreasing part of the experimental rate curves was considered for the numerical fitting procedure.

Experimental conditions	ϕ_{pre} (mol.m^{-2}.s^{-1})	b (number.m^{-1})
850°C in 20% O_2 – 80% N_2	$3.8\ 10^{-9} \pm 0.4\ 10^{-9}$	$1.8\ 10^{4} \pm 0.4\ 10^{4}$
850°C in 5% O_2 – 5% N_2 – 90% He	$3.9\ 10^{-9} \pm 0.2\ 10^{-9}$	$2.3\ 10^{4} \pm 0.2\ 10^{4}$

Table 2. Values of ϕ_{pre} and b parameters and their corresponding variation range.

Kinetics of nucleation and growth of nodules

The two parameters that model the part of the reaction rate due to the nucleation and growth of nodules are ϕ_{post}, which is the areic growth rate of the nodules, and γ□□, which is the areic nucleation frequency of the nodules. Other model parameters ($S_m(t)_{post}$ and $S_L(t)/S$) are linked to these two parameters (see Table A and B in Appendix). Parameters γ and ϕ_{post} were adjusted in order to account for the whole set of experimental curves. In the case of 5% O_2 – 5% N_2 - 90% He, it was possible to determine the value of ϕ□$_{post}$ with a low uncertainty. Actually, to model the asymptotical value of the experimental curves, the ϕ_{post}□ parameter must be set to □approximately 5.2 10^{-4} mol.m^{-2}.s^{-1}. In the case of 20% O_2 – 80% N_2 mixture, it was possible to get the value of ϕ□$_{post}$ using the ratio $\phi(P_{O2} = 5\ kPa)/\phi(P_{O2}\ init = 20\ kPa)$ (whose value is around 0.55, see Figure 6) and the value of ϕ□$_{post}$ obtained for 5% O_2 – 5% N_2 - 90% He mixture (5.2 10^{-4} mol.m^{-2}.s^{-1}). It leads to a value of ϕ□$_{post}(P_{O2} = 20\ kPa)$ equal to 9.5 10^{-4} mol.m^{-2}.s^{-1}. As the kinetic data are not reproducible in the post-transition period, each curve can be simulated with a different value of the γparameter. Its mean value as well as its uncertainty range for both experimental conditions is reported in Table 3. The computed mass gain rates (in red) as well as the whole set of experimental curves (in black) are plotted in

Figure 10 for 20% O_2 - 80% N_2 and in Figure 11 for 5% O_2 - 5% N_2 - 90% He. γ and ϕ_{post} parameters used to compute the mass gain rates plotted in continuous red line in Figure 10 and 11 are the mean values given in Table 3. For the dotted red lines, the minimum and maximum values of γ reported in Table 3 have been used.

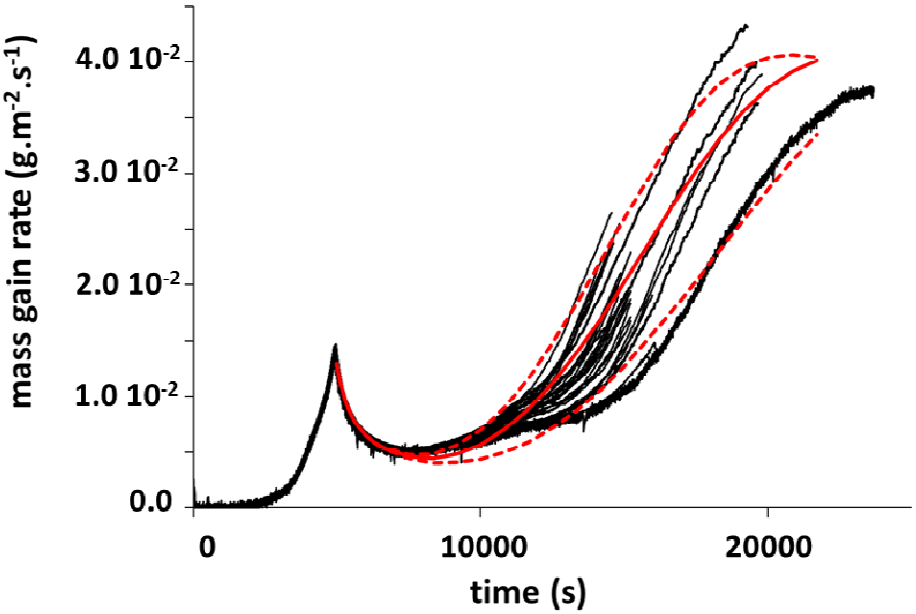

Fig. 10. Experimental (black lines) and calculated (red lines) mass gain rate vs. time at 850°C in 20% O_2 - 80% N_2. The ϕ_{post} parameter used to compute the mass gain rates is the mean value reported in Table 3. The γ parameter is either the mean value (continuous red line) or the lower/upper limit of the uncertainty range (dotted red lines).

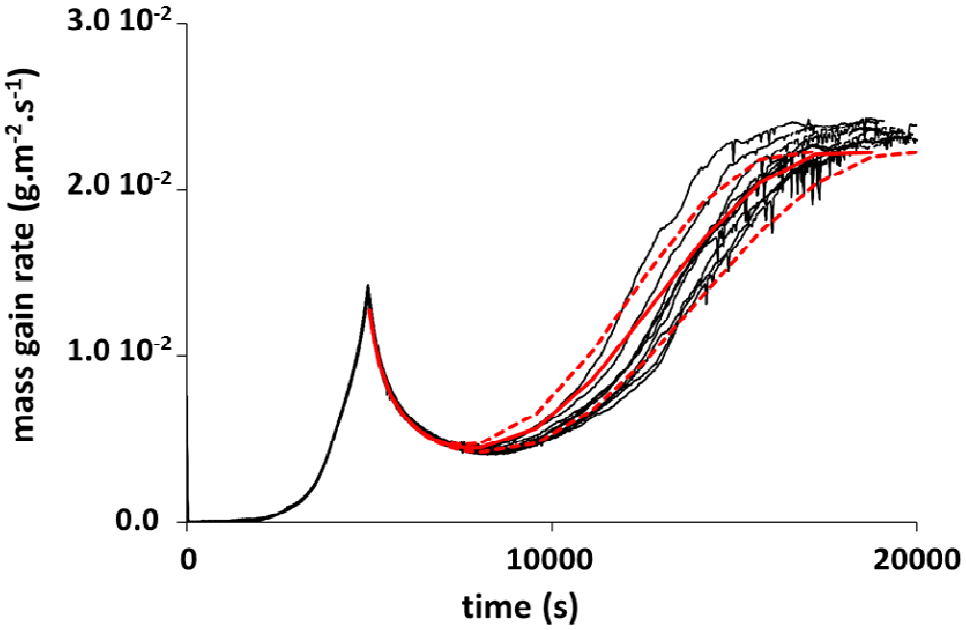

Fig. 11. Experimental (black lines) and calculated (red lines) mass gain rate vs. time at 850°C in 5% O_2 - 5% N_2 - 90% He. The ϕ_{post} parameter used to compute the mass gain rates is the mean value reported in Table 3. The γ parameter is either the mean value (continuous red line) or the lower/upper limit of the uncertainty range (dotted red lines).

Experimental conditions	γ(nb.m^{-2}.s^{-1})	ϕ_{post} (mol.m^{-2}.s^{-1})
850°C in 20% O_2 – 80% N_2	$2.1\ 10^3 \pm 1\ 10^3$	$9.5\ 10^{-4} \pm 0.7\ 10^{-4}$
850°C in 5% O_2 – 5% N_2 – 90% He	$1.8\ 10^4 \pm 0.6\ 10^4$	$5.2\ 10^{-4} \pm 0.2\ 10^{-4}$

Table 3. Values of γ and ϕ_{post} and their corresponding variation range.

The values of γ obtained for low and high oxygen and nitrogen partial pressures confirm that the lowest partial pressures conditions favour the appearance of nodules rather than their growth. It can be seen in Figure 11 that at the end of the accelerated period the kinetic regime is approximately linear (constant rate); moreover, the various curves reach the same asymptotical value. Such a linear regime corresponds to a situation where all nodules have merged, thus resulting in a constant value of the $S_m(t)_{post}$ function. In the case of experiments in 20%O_2 - 80%N_2 mixture the linear period is not so clearly visible due to a lower frequency of nucleation.

The non-reproducibility of the rate curves in the post-transition stage is easy to explain from statistical considerations; the number of nodules appearing randomly on the surface during an experiment remains relatively small compared to what happens in the case of powders which display a very high surface area.

4.2. Mechanism of nodules growth

Reactions sequence during the post-transition stage

The specimens were characterized with various techniques [10][12]: optical microscopy, scanning electron microscopy, X-ray tomography, energy dispersive X-ray spectrometry with silicon drift detector, high temperature X-ray diffraction, secondary ion mass spectrometry as well as Raman spectrometry. Figure 12 shows a typical oxide microstructure during the post-transition period and the corresponding scheme of the reaction zones to consider in order to understand which reactions could explain the growth of a nodule. In the regions containing nodules, going from the external surface to the inner metallic phase, successive zones are distinguished: a cracked (initially dense) zirconia layer permeable to gases, a “porous” zirconia layer, a layer containing both dense zirconia and ZrN precipitates (gold colour), the metallic part with the α-Zr(O) phase and the bulk alloy (α-Zr). The same succession of phases and interfaces was observed whatever the size of the nodules, independently of time and space.

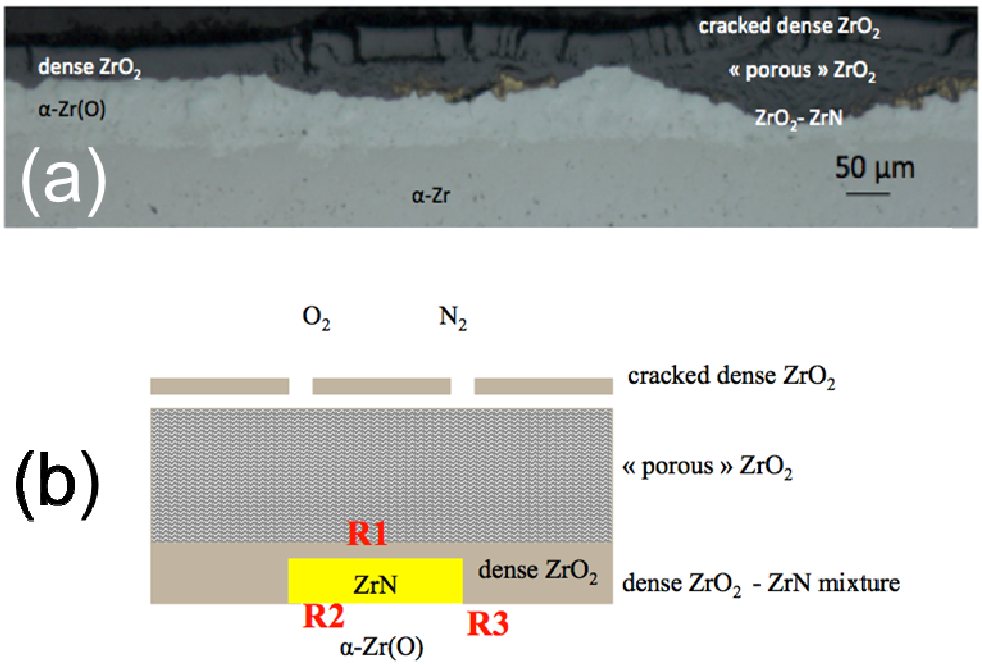

Fig. 12. Optical microscopy image of a Zircaloy-4 plate cross section in the post-transition stage after reaction at 850°C in 20% O_2 - 80% N_2 mixture (a) and scheme of the reaction zone in a growing nodule (b).

Due to the presence of large cracks in the outermost zirconia layer, the reacting gases have a direct access to the porous zirconia layer. On the basis of the kinetic model described in section 4, it can be inferred that the growth of a nodule corresponds to the inward advance of the two-phase layer (dense ZrO_2 – ZrN mixture) at the expense of the metallic phase. As shown by Steinbrück, nitrogen may react with α-Zr(O) to form a two-phase mixture of oxide and nitride [19]. Thus, to explain the advance of the oxide/metal interface, the following reactions taking place near the metal/oxide interface can be proposed:

$$ZrN + O_2 = N^* + ZrO_2 \qquad (R1)$$

$$N^* + ZrO_x = ZrN + xO^* \qquad (R2)$$

$$(2-x)O^* + ZrO_x = ZrO_2 \qquad (R3)$$

where ZrO_x is the notation used for the α-Zr(O) phase.

Reaction R1 corresponds to the oxidation of ZrN precipitates into dense zirconia by oxygen which is assumed to reach the reaction zone as a molecular specie. This reaction releases nitrogen species, probably present as point defects in ZrN (noted N^*) which diffuse inwards and react according to R2 with the α-Zr(O) phase to give new ZrN precipitates. The oxygen released by the reaction R2 (noted O^*) reacts with the α-Zr(O) phase leading to the formation

of dense zirconia in the two-phase layer. ZrN can be seen as a catalyst for zirconium oxidation since it offers a new reaction path without changing the reaction balance. Then, the transport of gases through the cracks initiated into the first dense zirconia scale allows setting up an auto-catalytic mechanism, which self-sustains the formation of zirconium nitride and dense zirconia at metal-oxide interface.

Oxidation and nitriding reactions are at the origin of the "porosity" observed in the post-transition oxide layer. SEM images show that cracks along the zirconium nitride precipitates are parallel to the metal-oxide interface [10]. As depicted by Figure 13-A, the nitridation of α-Zr(O), which occurs without volume change, leads to a two-phase ZrN/ZrO_x layer. The oxidation of the α-Zr(O) phase into dense zirconia (Figure 13-B) leads to a volume increase (the Pilling and Bedworth ratio $PBR_{ZrO2/Zr}$ is 1.56) which induces tensile stresses on ZrN and cracks. The ZrN precipitates are finally oxidised and, as this reaction leads to a volume increase ($PBR_{ZrO2/ZrN}$= 1.47), the dense zirconia located near to the metal-oxide interface, and in contact with ZrN, is submitted to tensile stresses which generate cracks (Figure 13-C). These phenomena explain the increase of the porous zirconia layer thickness while the nodule grows inwards the alloy.

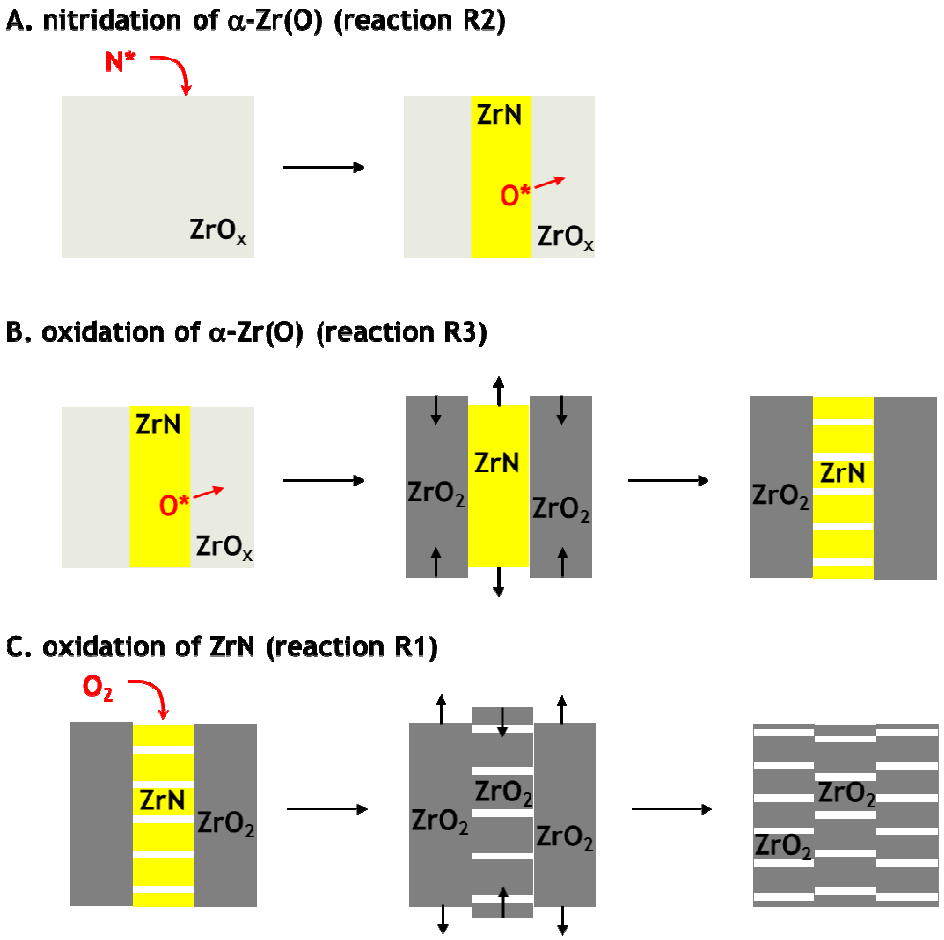

Fig. 13. Scheme of stresses (arrows) and cracks (white lines) generated during the creation (A, B) and the oxidation (C, D) of ZrN precipitates.

Rate-determining step of nodules growth

From previous sections (3. and 4.1.), we know that, despite of its complexity, a steady-state is established during the post-transition stage, which is kinetically controlled by a single rate-determining step located near the mobile oxide/metal interface. This excludes (at least in the experimental conditions settled for this study) a possible limitation by gas diffusion through the cracked and porous zirconia layers situated above the two-phase layer (no starvation). The problem now is to determine the exact nature of the rate-determining step and the expression of the areic growth rate $\phi(T,P_i)_{post}$. The whole mechanism must involve the mechanisms of each of the reactions R1, R2 and R3. It was shown in section 3.3. that the oxygen partial pressure has an accelerating influence on the nodules growth. It can thus be deduced that the rate-determining step should belong to reaction R1 which is the only one that involve gaseous oxygen. In addition, the localization of the rate-determining step at the mobile oxide-metal

interface is consistent with reaction R1 since the two-phase layer where this reaction takes place spreads along the metal phase and can be regarded as “mobile” with time.

The series of elementary steps proposed to describe the mechanism of zirconia growth by zirconium nitride oxidation are given in Table 4. The various steps involve distinct reaction intermediates which are surface sites s, adsorbed oxygen O-s, zirconia oxygen vacancies $V_O^{\bullet\bullet}$, free electrons (for charge compensation), interstitial $N_{i(ZrN)}$ (release of nitrogen which diffuses inwards through ZrN). In addition, reaction R2 and R3, which can be considered at equilibrium (due to the rate-determining step approximation), can be rewritten as follows:

$$Zr^{\times}_{Zr(\alpha-Zr)} + xO_{i(\alpha-Zr)} + N_{i(ZrN)} = Zr^{\times}_{Zr(ZrN)} + N^{\times}_{N(ZrN)} + xO_{gb} \qquad (R2')$$

$$Zr^{\times}_{Zr(\alpha-Zr)} + xO_{i(\alpha-Zr)} + (2-x)O_{gb} = Zr^{\times}_{Zr(ZrO_2)} + 2O^{\times}_{O(ZrO_2)} \qquad (R3')$$

where $O_{i\text{-}(\alpha\text{-}Zr)}$ represents an oxygen atom in the α-Zr(O) phase and O_{gb} an oxygen atom at a grain boundary in the two-phase layer.

It can be noticed that a linear combination of the steps 1-4 and reactions R2’ and R3’ such as $\left(1-\frac{x}{2}\right)\left[(1)+2[(2)+(3)]+(4)+(R2')+\frac{x}{2-x}(R3')\right]$ leads to the stoichiometric reaction balance:

$$\left(1-\frac{x}{2}\right)O_2(g) + ZrO_x \xrightarrow{ZrN} ZrO_2 \qquad (R4)$$

The equilibrium constant of the global reaction (R4), *K*, is related to the equilibrium constants of the intermediate reactions K_i (*i= 1, 2, 4, R2’* and *R3’*) by:

$$K^{\frac{2}{2-x}} = K_1 K_2^2 K_4 K_{R2'} K_{R3'}^{x/2-x} \qquad (Eq.\ 6)$$

It is possible to express the areic growth rate by solving a system of equations corresponding to the proposed mechanism. The deviation from equilibrium was not considered here due to the chosen experimental conditions. Theoretical expressions of the ϕ_{post} function can be computed assuming that one of the elementary steps (1, 2 or 4) is rate-determining. The corresponding expressions have been reported in the last column of Table 4. It can be shown in Figure 6 that the experimental variations of the areic growth rate with the oxygen partial pressure can be very well adjusted by the following law (continuous line):

$$a\frac{\sqrt{P(O_2)}}{1+b\sqrt{P(O_2)}} \qquad \text{(Eq. 7)}$$

with a= 2.3 and b=0.06.

This result demonstrates that the rate-determining step is the external interface step of the reaction of ZrN oxidation with coefficient a corresponding to $k_2\sqrt{K_1K_4K_{R2'}K_{R3'}^{x/2-x}}$ and coefficient b to $\sqrt{K_1}$. It can also be noticed that the expression of ϕ_{post} is in agreement with the absence of influence of the nitrogen partial pressure.

So it can be concluded that the reaction sequence based on an auto-catalytic effect of ZrN precipitates is able to quantitatively explain the variations of the rate with the partial pressure of the gases, due to an interfacial rate-determining step involved in the mechanism of oxidation of zirconium nitride precipitates, and in agreement with the $S_m(t)_{post}$ kinetic modelling.

Elementary step		Areic growth rate ϕ_{post}
1 - Adsorption step	$O_2 + 2s = 2O - s$	$\phi_1 = k_1P(O_2)\frac{K_2^2K_4K_{R2'}K_{R3'}^{x/2-x}}{1+K_2\sqrt{K_4K_{R2'}K_{R3'}^{x/2-x}}}$
2 - External interface step	$O - s + V_O^{\bullet\bullet} + 2e' = O_{O(ZrO_2)}^{\times} + s$	$\phi_2 = k_2\frac{\sqrt{P(O_2)}}{1+\sqrt{K_1P(O_2)}}\sqrt{K_1K_4K_{R2'}K_{R3'}^{x/2-x}}$
3 - Diffusion step	$V_O^{\bullet\bullet}$, e' and $O_{O(ZrO_2)}^{\times}$ from the internal interface to the external interface	-
4 - Internal interface step	$Zr_{Zr(ZrN)}^{\times} + N_{N(ZrN)}^{\times} = Zr_{Zr(ZrO_2)}^{\times} + 2V_O^{\bullet\bullet} + 4e' + N_{i(ZrN)}$	$\phi_4 = k_4$

Table 4. Mechanism of ZrN oxidation (reaction R1) and expression of the areic growth rate of zirconia.

5. Conclusions

This study proposes for the first time a quantitative modelling of the oxidation of Zircaloy-4 in oxygen and nitrogen mixtures. Thermogravimetry experiments were done with thin plates and variations of the reaction rate with time and partial pressures of both gases were investigated at 850°C. Dedicated experiments allowed attesting the existence of a steady-state and a rate-determining step during the post-transition stage. The validation of both assumptions has enabled us to write the reaction rate as the product of two functions: the areic growth rate $\phi(T,P_i)$ and the function of time $S_m(t)$. The separate influence of the oxygen and nitrogen partial pressures on the ϕ function was experimentally determined with the jump method which allows exploring the kinetic behaviour of a reacting system at a given extent of reaction.

Based on detailed observations of oxidised specimens, a nucleation and growth model originally derived for reactions with powders was successfully applied for the random appearance and growth of zirconia nodules from the surface towards the inner bulk alloy. Four functions are then necessary to model the reaction rate: $S_m(t)_{pre}$ and $\phi(T,P_i)_{pre}$ functions that describe growth of dense zirconia and $S_m(t)_{post}$ and $\phi(T,P_i)_{post}$ that describe nodules growth. The nucleation and growth model was able to well reproduce the shape of the rate curves versus time during the post-transition stage and to explain the non-reproducibility of the experiments. With such a model, the localization of the rate-determining step of nodules growth was identified as being located at the oxide-metal interface. Moreover, values for the set of parameters (the growth rate of dense zirconia ϕ_{pre}, the number of barriers per unit length b, the nodules growth rate ϕ_{post} and the areic nucleation frequency γ) could be obtained from curve fitting.

From the arrangement of the various phases and interfaces between phases in the nodules (porous zirconia, two-phase ZrN and dense ZrO_2 layer, α-Zr(O)), it was possible to propose a sequence of three reactions:

- R1: oxidation of ZrN precipitates present at the oxide-metal interface into dense zirconia by oxygen molecules,
- R2: nitridation of α-Zr(O) by nitrogen atoms released in R1,
- R3: oxidation of α-Zr(O) by oxygen atoms released in R2.

The porosity of the zirconia layer in the growing nodules can be explained by the volume changes associated to reactions R1 and R3 leading to local stresses and cracks.

Finally, a mechanism decomposed in elementary steps for the oxidation of zirconium nitride precipitates was proposed to explain the variations of the areic growth rate ϕ_{post} with oxygen and nitrogen partial pressures and to precise the nature of the rate-determining step. The external interfacial reaction step of the oxidation of the ZrN precipitates was found to control the nodules growth during the post-transition stage.

Due to the number of experiments carried out to validate the assumptions (existence of a steady-state and of a rate determining step), to determine the functions necessary to model the reaction rate and to characterize the oxide scale, only one temperature was investigated. It would be of great interest to determine the effect of temperature on processes (nodules appearance and growth) by performing thermogravimetry tests at different temperatures. The number of experimental tests would be lower if the assumptions are assumed to remain valid when temperature changes. It would be also interesting in further work to investigate the dependency of the nucleation frequency (nodules appearance frequency) with the oxygen and nitrogen partial pressure. Finally, it would be worth determining the influence of the geometry (cylindrical instead of plate) on the function of time $S_m(t)_{post}$.

The model presented in this paper provides an explanation of the accelerating effect of nitrogen by the nucleation and growth of nodules. The mass gain rate can then be well reproduced by calculating integrals. It seems complicated to make such computations in code systems for simulation of nuclear accidents. Nevertheless, the complex model could be simplified in order to have a simple formulation for the mass gain rate, such as “an accelerated law” as proposed in [7]. In this formulation, only one parameter, the accelerated rate constant, is required to compute the mass gain rate. The accelerated rate constant is temperature dependent with the temperature dependence usually following Arrhenius' equation. This study demonstrates that the rate constant not only depends on the temperature but also also on the partial pressures. The next step is thus to compute this accelerated rate constant from the set of parameters of the complex model (ϕ_{pre}, b, ϕ_{post} and γ) for different conditions (temperature and gas partial pressures). With this simple model, it will be possible to compute accidental scenarios with air ingress, taking the accelerated rate constant suitable for the conditions encountered during the transient.

Appendix A

The calculation method, as proposed by Delmon [15] is based on a statistical approach (random surface nucleation with a constant frequency) and accounts for the possible

recovering of the growing nuclei. The expressions of the function $S_m(t)_{post}$ are given in Table A.

List of notations

γ: areic nucleation frequency in number.m^{-2}.s^{-1}

e_0: half-thickness of the plate in m

k: increasing rate of the radius of the semi-ellipsoidal shape of a post-transition zone in m.s^{-1}

$V_m(Zr)$: molar volume of zirconium in m^3.mol^{-1}

x: distance between the surface of the plate and the inner plane in m (cf. Fig A.1)

A is defined by Eq. A.1 :

$$A = \frac{\pi e_0^3 \gamma}{k} \qquad \text{(Eq. A.1)}$$

τ is a dimensionless time variable and ξ corresponds to the dimensionless time of appearance of the nodules:

$$\tau = \frac{k}{e_0} t \qquad \text{(Eq. A.2)}$$

$$\xi = \frac{x}{e_0} \qquad \text{(Eq. A.3)}$$

The relationship between k and ϕ_{post} is given by Eq. A.4 where $V_m(Zr)$ is the molar volume of zirconium in m^3.mol^{-1}:

$$k = \phi_{post} V_m(Zr) \qquad \text{(Eq. A.4)}$$

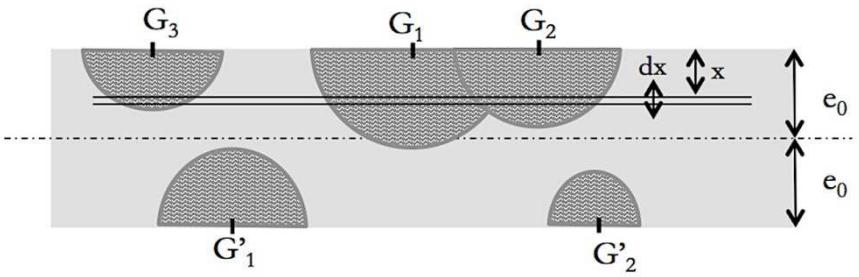

Fig. A.1. Inward growth of nuclei from the surface of the plate intersecting a plane at a distance x from the surface [15]

$0 \le \tau \le 1$
$S_m(\tau)_{post} = \frac{V_m(Zr)}{e_0} A \exp\left(-\frac{A}{3}\tau^3\right) \int_0^{\tau} \left[\left(\tau^2 - \xi^2\right) \exp\left(\frac{A}{3}\xi^2(3\tau - 2\xi)\right) \right] d\xi$
$1 \le \tau \le 2$
$S_m(\tau)_{post} = \frac{V_m(Zr)}{e_0} A \exp\left(-\frac{A}{3}\tau^3\right) \int_0^{2-\tau} \left[\left(\tau^2 - \xi^2\right) \exp\left(\frac{A}{3}\xi^2(3\tau - 2\xi)\right) \right] d\xi$ $+ \frac{V_m(Zr)}{e_0} 2A \exp\left(-\frac{2A}{3}\left(\tau^3 - 6\tau + 8\right)\right) \int_{2-\tau}^{1} \left(\tau^2 - \xi^2 + 2\xi - 2\right) \exp\left(2A\xi(\xi - 2)(\tau - 2)\right) d\xi$
$\tau \ge 2$
$S_m(\tau)_{post} = \frac{V_m(Zr)}{e_0} 2A \exp\left(-\frac{2A}{3}\left(\tau^3 - 6\tau + 8\right)\right) \int_0^{1} \left(\tau^2 - \xi^2 + 2\xi - 2\right) \exp\left(2A\xi(\xi - 2)(\tau - 2)\right) d\xi$

Table A. Equations of the function $S_m(\tau)_{post}$ for the nucleation and growth of nodules.

Appendix B

The expressions used for the calculation of $S_L(\tau)$ are given in Table B for the three periods of the dimensionless time τ (cf. Appendix A). Details on the calculations may be found in [12].

$0 \le \tau \le 2$
$\frac{S_L(\tau)}{S} = \exp\left(-\frac{A}{3}\tau^3\right)$
$\tau \ge 2$
$\frac{S_L(\tau)}{S} = \exp\left(-\frac{2A}{3}\left(\tau^3 - 6\tau + 8\right)\right)$

Table B. Equations of the function $S_L(\tau)/S$ for the nucleation and growth of nodules.

References

[1] E.T. Hayes and A.H. Roberson, J. Electrochem. Soc. 96, 142 (1949).

[2] E.B. Evans, N. Tsangarakis, H.B. Probst and N.J. Garibotti, Proceedings of the Conference on Metallurgical Society of AIME, Symposium on High Temperature Gas-Metal Reactions in Mixed Environments, Boston, May 9-10 1972, 248.

[3] C.J. Rosa and W.W. Smeltzer, Zeitschrift Fur Metallkunde 71, 470 (1980).
[4] K. Natesan and W. K. Soppet, Air Oxidation Kinetics for Zr-based Alloys, Argonne National Laboratory Report 03/32, NUREG/CR-6846, June 2004.
[5] C. Duriez, T. Dupont, B. Schmets et F. Enoch, J. Nucl. Mater. 380, 30 (2008).
[6] M. Steinbrück, J. Nucl. Mater. 392, 531 (2009).
[7] O. Coindreau, C. Duriez and S. Ederli, J. Nucl. Mater. 405, 207 (2010).
[8] M. Steinbrück and M. Böttcher, J. Nucl. Mater. 414, 276 (2011)
[9] I. Idarraga, M. Mermoux, C. Duriez, A. Crisci and J.P. Mardon, J. Nucl. Mater. 421, 160 (2012).
[10] M. Lasserre, O. Coindreau, M. Pijolat, V. Peres, C. Duriez and J-P. Mardon, to be published in J. Mater. and Corr. 64, DOI: 10.1002/maco.201307078 (2013).
[11] M. Pijolat and M. Soustelle, Thermochimica Acta 478, 34 (2008).
[12] M. Lasserre, Modélisation des phénomènes de corrosion du Zircaloy-4 sous mélanges oxygène-azote à haute température, phD thesis, Ecole des Mines de St Etienne (2013).
[13] P. Glansdorff and I. Prigogine, Thermodynamic Theory of Structure, Stability and Fluctuations, Wiley (1971).
[14] K. L. Mampel, Z. Phys. Chem. A 187, 235 (1940).
[15] B. Delmon, Introduction à la cinétique hétérogène, Editions Technip, Paris (1969).
[16] M. Tupin, Approfondissement des mécanismes d'oxydation de deux alliages de Zirconium : Zircaloy-4 et ZrNbO, sous oxygène et sous vapeur d'eau. Comparaison des régimes cinétiquement limitants, phD thesis, Ecole des Mines de Saint-Etienne (2002).
[17] M. Tupin, F. Valdivieso, M. Pijolat, M. Soustelle, A. Frichet and P. Barberis, Materials Science Forum, 461-464, 139 (2004).
[18] J.K. Dawson, G. Long, W.E. Seddon and J.F. White, J. of Nucl. Mater. 25, 179 (1968).
[19] M. Steinbrück, J. Nucl. Mater. 447 (2014) pp. 46-55.